Sensors and Actuators B 228 (2016) 515–522

Contents lists available at ScienceDirect

Sensors and Actuators B: Chemical

journal homepage: www.elsevier.com/locate/snb

Highly selective detection of trace hydrogen against CO and CH_4 by $Ag/Ag_2O–SnO_2$ composite microstructures

Hui-Hui Li, Yi He, Pan-Pan Jin, Yang Cao, Mei-Hong Fan, Xiaoxin Zou, Guo-Dong Li*

State Key Laboratory of Inorganic Synthesis and Preparative Chemistry, International Joint Research Laboratory of Nano-Micro Architecture Chemistry, College of Chemistry, Jilin University, 2699 Qianjin Street, Changchun 130012, China

ARTICLE INFO

Article history:
Received 19 August 2015
Received in revised form 14 January 2016
Accepted 18 January 2016
Available online 21 January 2016

Keywords:
$Ag/Ag_2O–SnO_2$
Composite
Porous
Hydrogen
Gas sensor

ABSTRACT

Both response and selectivity are key issues for a gas sensing material. Here, we presented a porous $Ag/Ag_2O–SnO_2$ composite with excellent sensing performance towards hydrogen. The optimal weight ratio of Ag to SnO_2 was 3 wt% in the $Ag/Ag_2O–SnO_2$ composite, which gave the highest response of 40–200 ppm hydrogen at 170 °C. And what is more, it was nearly insensitive to carbon monoxide and methane at this temperature. The porous microspheres composite exhibited high response and rapid response (less than 5 s) to trace amount of hydrogen. The high response and excellent selectivity of this composite could be attributed to the high catalytic activity of Ag/Ag_2O nanoparticles built on the surface of SnO_2 microspheres, the Schottky barrier and low working temperature.

1. Introduction

To deal with the challenge brought by the ever growing energy crisis, tremendous efforts have been made on the exploitation of alternative energy sources and the efficient utilization of all kinds of fossil fuels [1]. Coal and petroleum, the most important fossil energy carrier, are widely used in the world. While, hydrogen (H_2) accompanied with carbon monoxide (CO), derived from coal gasification and steam methane reformation (SMR), can not only be used as energy carrier, but also the important reactant for chemical works [2–4]. Especially, hydrogen has been widely used in various industries including petroleum refining processes, the synthesis of ammonia and methanol, biological systems, transportation, aerospace, fuel cells and automotive industries [5–8]. Furthermore, H_2 and CO can also be used in metallurgical industry due to their high reducing activity at suitable temperature [9–13]. However, hydrogen will form explosive mixture with air in a wide volume range of 4–75% [14]. And what's more, the diffusion and permeability rate of hydrogen is also very high. To prevent explosive accidents, it is necessary to detect hydrogen at low concentration. However, it is still a challenge to selectively detect hydrogen and carbon monoxide/methane due to their remarkable similarity in react activity [15,16].

In recent years, metal oxide semiconductors (MOS), including cuprous oxide (Cu_2O), tungsten oxide (WO_3), indium oxide (In_2O_3), zinc oxide (ZnO), titanium oxide (TiO_2) and tin oxide (SnO_2), are considered as promising materials for efficient gas detection because of the convenience, simplicity, cost-economy, reliability and structural diversity [17–34]. In particular, SnO_2, an important n-type semiconductor with wide direct band gap (E_g = 3.6 eV, at 300 K), exhibits high conductivity, tunable structure and good chemical stability. It has been widely used to detect reducing gases, such as CH_4, CO and H_2 [16,35–37]. For example, SnO_2 nanowires based sensors show response to both H_2 and CO at room temperature accompanied with long response and recovery time [16]. Wang et al. reported a p-NiO/n-SnO_2 heterojunction nanofiber composite for the detection of hydrogen at 320 °C [35]. Kunitake et al. synthesized a nanotubular SnO_2 gas sensor exhibiting superior response toward H_2 and CO at high working temperature (*i.e.*, 450 °C) [36]. However, most of the previous SnO_2 based gas sensors worked at relatively high temperature and showed poor selectivity to H_2, CO and methane. Furthermore, the lower the working temperature is, the less energy will be consumed, and the longer the sensor life will be.

Although some works have been reported using Ag as a catalytic dopant on the surface of SnO_2 to improve its hydrogen detecting performance [38–40], the working temperature is rather high. Here, we report Ag/Ag_2O decorated porous SnO_2 microsphere composites with good selectivity to H_2 at a relatively low working temperature (*i.e.*, 170 °C). The sensors fabricated by the above com-

* Corresponding author.
E-mail addresses: lgd@jlu.edu.cn, lifind@21cn.com (G.-D. Li).

http://dx.doi.org/10.1016/j.snb.2016.01.078
0925-4005/

posites showed high response and short response time (less than 5 s) towards H_2 and nearly insensitive to CO and CH_4 at the same condition. A sensing mechanism was also proposed for its high response, good selectivity and low working temperature.

2. Experimental

2.1. Chemicals and reagents

Stannic chloride pentahydrate ($SnCl_4{\cdot}5H_2O$) was purchased from Tianjin Fuchen Chemical Reagent Factory. Isopropanol, silver nitrate ($AgNO_3$) and ethanol were purchased from Beijing Chemical Works. Glycerol was purchased from Sinopharm Chemical Reagent Co., Ltd. All the above chemicals were of analytical grade and used without further purification. Deionized water (18.2 MΩ·cm) was used for all the experiments.

2.2. Synthesis and characterizations of porous Ag/Ag_2O–SnO_2 composite

Porous SnO_2 microspheres were prepared by a solvothermal method. In a typical synthesis procedure, 350 mg of $SnCl_4{\cdot}5H_2O$ (1 mmol) was dispersed in a mixed solution containing 8 mL glycerol and 30 mL isopropanol. The mixture was transferred into a 60 mL Teflon-lined autoclave, which was then heated at 180 °C for 12 h. After cooling to room temperature naturally, the resulting precipitate was centrifuged and washed thoroughly with ethanol several times. The precipitate was then dried at 80 °C in air, leading to the formation of porous SnO_2 precursor. Porous Ag/Ag_2O–SnO_2 composites were prepared by an impregnation method [41]. Typically, 134 mg of the obtained porous SnO_2 was added in 2 mL ethanol containing different amount of $AgNO_3$ (2.2, 6.7, 13.4 and 18.9 mg) and stirred at room temperature for 2 h. The mixture was dried at 80 °C, and then calcined at 500 °C for 2 h. The resulting products were denoted as Ag/Ag_2O–SnO_2—1 wt%, Ag/Ag_2O–SnO_2—3 wt%, Ag/Ag_2O–SnO_2—6 wt% and Ag/Ag_2O–SnO_2—9 wt%, where the number meant the weight percent of Ag species to SnO_2.

The structure and morphology of the final products were characterized with an X-ray diffractometer (XRD, Rigaku D/Max 2550 X-ray diffractometer using Cu Kα radiation operated at 200 mA and 50 kV), a field-emission scanning electron microscope (FE-SEM, JEOL JSM 6700F electron microscope) and a field-emission transmission electron microscope (FE-TEM, Philips-FEI Tecnai G2S-Twin). The composition and chemical state of these composites were obtained on an X-ray photoelectron Spectroscopy (XPS, ESCALAB 250 X-ray photoelectron spectrometer). BET surface area and the corresponding Barrett–Joyner–Halenda (BJH) pore diameter were measured by using a Micromeritics ASAP 2020M system. And the work function was measured by using the Scanning Kelvin Probe (SKP 5050).

2.3. Sensor fabrication and testing

The sensors were fabricated by pasting viscous slurry, composed of the composites and small amount of ethanol, onto a ceramic tube which was positioned with a pair of Au electrodes and four Pt wires on both ends of the tube. The operating temperature of the sensor was controlled by the nickel–chromium heating wire located in the center of the tube (as shown in Scheme 1A and C). All the sensors were fabricated in exactly the same manner except the composite. To ensure the good contact between the sensing material and the Au electrodes, the as-fabricated sensors were aged at 200 °C for 12 h. Gas sensing tests were performed on a commercial CGS-8 Gas Sensing Measurement System (Beijing Elite Tech Company Limited).

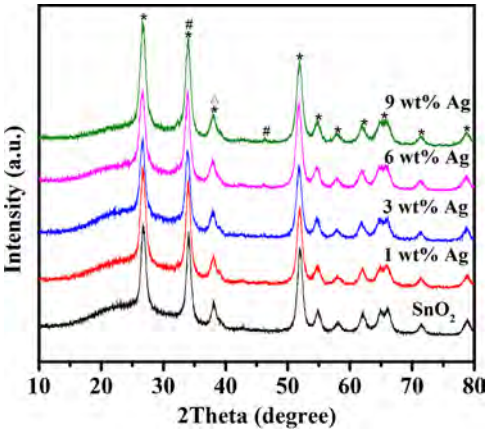

Fig. 1. The XRD patterns of porous SnO_2, Ag/Ag_2O–SnO_2—1 wt%, Ag/Ag_2O–SnO_2—3 wt%, Ag/Ag_2O–SnO_2—6 wt% and Ag/Ag_2O–SnO_2—9 wt%. The peaks corresponding to SnO_2 are marked with "∗", to Ag are marked with "△" and to Ag_2O are marked with "#".

Gas sensing performances were evaluated by a static test system including a one-liter chamber with a few pieces of aluminum foil. In the testing system (Scheme 1B), a load resistor with a known resistance (R_L) is connected in series with the sensor to determine the resistance variation of the sensor. And the sensor response is defined as R_a/R_g, where R_a is the sensor resistance in air and R_g is that in target gas at the same operating temperature. During the sensing test, the operating temperature is in the range of 130–260 °C, and the relative humidity is around 25% at room temperature (27 °C). A typical testing procedure was as follow: to obtain 200 ppm hydrogen in air, 200 μL hydrogen was injected into the testing chamber containing fresh air (~1 L) with a stopper by a microsyringe and shaken for about 10 min. Then, the sensor accompanied with a stopper was put into the testing chamber to get R_g. Then the sensor was exposed to fresh air again for recovery.

3. Results and discussion

As illustrated in Scheme 2, the porous Ag/Ag_2O–SnO_2 microspheres were prepared by an impregnation method using porous SnO_2 as precursor. The structure and composition of the precursor and Ag/Ag_2O-loaded porous SnO_2 microsphere composites were determined by XRD (Fig. 1). The diffraction peaks can be well indexed to tetragonal rutile SnO_2 (JCPDS card No. 41-1445), revealing the good crystallinity of the obtained products. No peaks related to Ag species present in the XRD patterns of Ag/Ag_2O–SnO_2—1 wt% and Ag/Ag_2O–SnO_2—3 wt% due to the trace amount of Ag in the composites. Further increasing the amount of Ag, the peaks related to Ag_2O (JCPDS No. 42-0874) can be observed, indicating the formation of crystallized Ag_2O on the surface of porous SnO_2. The diffraction peak of Ag is not appeared in the XRD pattern for the overlap between SnO_2 and Ag. In order to further confirm the chemical state of Ag species in the composites, XPS analysis was conducted for the final products. XPS survey spectrum of porous Ag/Ag_2O–SnO_2—3 wt% indicates the existence of Ag and Sn in the final product (Fig. S2). Although the distribution of the oxidation state of Ag is quite complicated due to the slight difference and other factors [42–44], it is clear that Ag^0 and Ag^+ coexisted in the product after carefully fitting the BE peak of Ag $3d_{5/2}$ in the high-resolution XPS spectra of Ag (Fig. 3). The peaks located at 368.2 eV and 367.7 eV can be attributed to the Ag^0 and Ag^+, respectively. In addition, Ag and Ag_2O nanoparticles with a size around 5 nanometers are also observed by HRTEM (Fig. 2D). The fringes with distance of 0.231 nm and 0.261 nm can be assigned to (1 1 1) plane of Ag

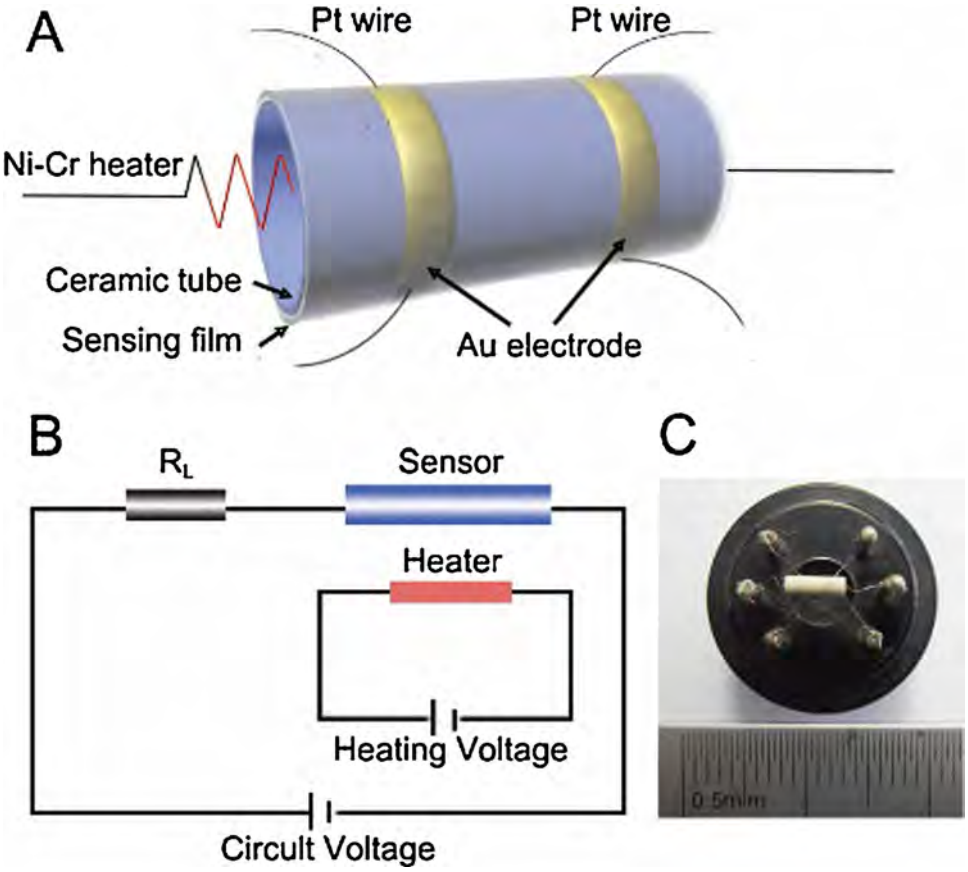

Scheme 1. (A) A diagram of the sensor composed of ceramic tube, two Au electrode, four Pt wires and a Ni–Cr wire. (B) A schematic diagram of the measurement circuit. (C) A photograph of a typical gas sensor.

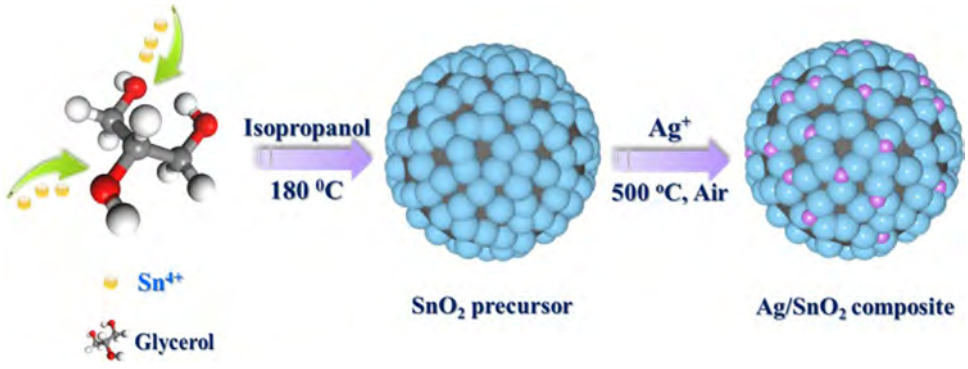

Scheme 2. Schematic representation for the formation of porous $Ag/Ag_2O–SnO_2$ composite.

[45] and (0 0 3) plane of Ag_2O [46], while the interplanar spacing of 0.338 nm is related to the (1 1 0) plane of SnO_2 [47].

As shown in Figs. 2(A and B) and S1 (A and B), the diameter of the spheres is about 1 μm for $Ag/Ag_2O–SnO_2$—3 wt% and SnO_2. The porous $Ag/Ag_2O–SnO_2$ composites are mainly composed of SnO_2 nanoparticles with sizes of around 10 nm according to the TEM image (Fig. 2C) and Sherrer equation based on XRD analysis.

Generally, surface area, one of the most important parameters for a porous material, is also responsible for the enhanced sensing performance of a gas sensor [48–50]. In this work, the porous structure and surface area of the products were studied by N_2 adsorption/desorption isotherm. As shown in Fig. 4, it is a typical type-IV isotherm with an H3-type hysteresis loop. The corresponding BJH pore-size distribution derived from the N_2 desorption isotherm is in the range of 2–50 nm, indicating the formation of mesoporous materials. The BET surface area of all the samples is as high as 34 $m^2 g^{-1}$ (Table S1). Owing to the large surface area and porous structure which favored gas molecular adsorption and diffusion, these materials give enhanced gas-sensing performance.

The H_2 sensing characters of these porous $Ag/Ag_2O–SnO_2$ composites and SnO_2 were evaluated systematically. The optimal operation temperature was determined according to the sensing response (R_a/R_g), response time and recovery time to 200 ppm H_2. As shown in Fig. 5A, although $Ag/Ag_2O–SnO_2$—6 wt% composite gave the highest response (R_a/R_g = 90) at 230 °C, it took much longer recovery time than $Ag/Ag_2O–SnO_2$—3 wt% (Fig. S3). What is more, it also shows remarkable response to CO at 230 °C (Fig. S6). Further increasing the amount of silver to about 9 wt%, the response is much lower than that of $Ag/Ag_2O–SnO_2$—3 wt% and other composites, indicating the optimal Ag content is 3 wt%. In order to

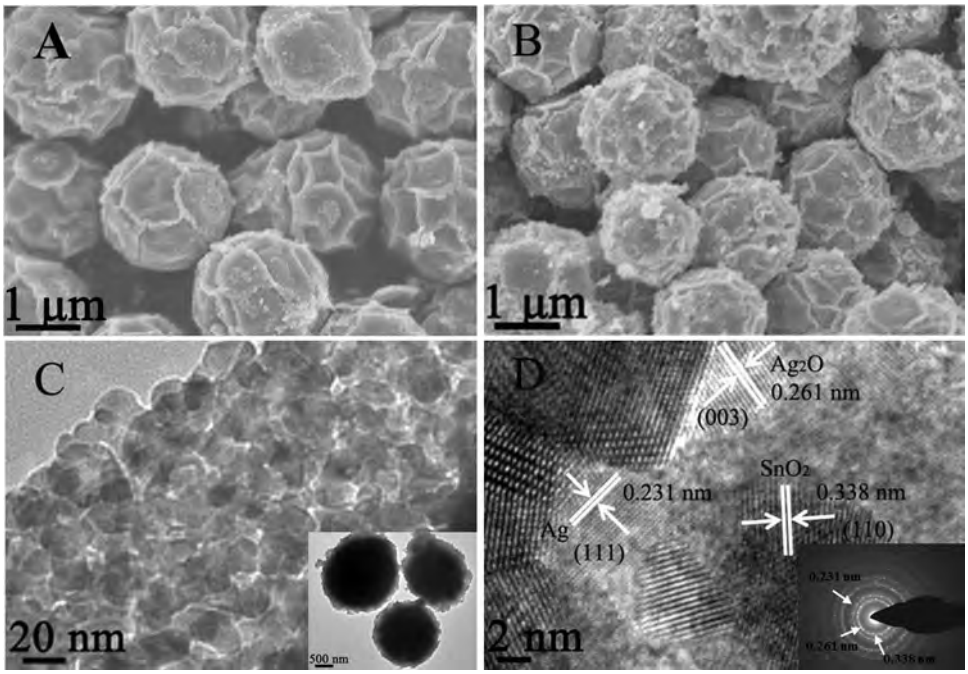

Fig. 2. SEM images of (A) porous SnO_2 and (B) Ag/Ag_2O–SnO_2—3 wt% composite, (C) TEM images, (D) HRTEM image and inset of (D) SAED pattern of Ag/Ag_2O–SnO_2—3 wt% composite.

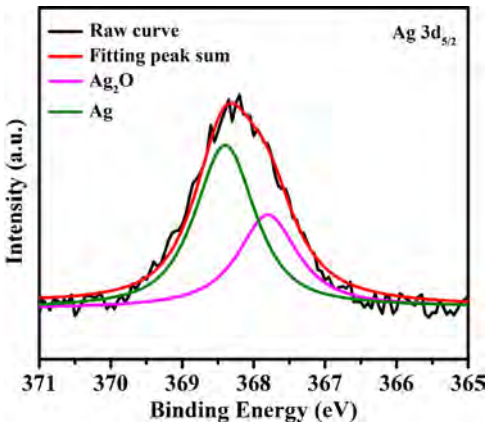

Fig. 3. High-resolution Ag $3d_{5/2}$ XPS spectra of Ag/Ag_2O–SnO_2—3 wt% composite.

investigate the relation between responses and the concentration of hydrogen, the responses of SnO_2, Ag/Ag_2O–SnO_2—3 wt% and Ag/Ag_2O–SnO_2—6 wt% to various concentrations of hydrogen were recorded at 170 °C (Fig. 5B). It is obvious that the response of Ag/Ag_2O–SnO_2—3 wt% and Ag/Ag_2O–SnO_2—6 wt% are much higher than that of porous SnO_2 spheres. While, as shown in Fig. S3A and B, with the increase of the Ag NPs content, the recovery time would be prolonged. Taking the lower silver content and lower working temperature into consideration, Ag/Ag_2O–SnO_2—3 wt% composite was studied in details. The response time for Ag/Ag_2O–SnO_2—3 wt% composite gas sensor is less than 5 s in the temperature range of 130–260 °C. Considering all the factors mentioned above, the optimal working temperature was determined as 170 °C due to the relatively high response (R_a/R_g = 40, 200 ppm hydrogen), rapid response (<5 s) and acceptable recovery time (93 s).

To further investigate the selectivity of this composite, the sensing responses towards 1–200 ppm CO and CH_4 were also obtained at 170 °C, respectively. As demonstrated in Fig. 6, Ag/Ag_2O–SnO_2—3 wt% composite exhibits the highest response of 40–200 ppm hydrogen, and nearly insensitive to CO and CH_4. To further confirm the good selectivity, the responses towards 100 ppm hydrogen, 100 ppm hydrogen together with 2000 ppm CO, 2000 ppm methane or both 2000 ppm CO and methane were measured at the same condition (Fig. S4). The responses are nearly the same, indicating the good selectivity towards hydrogen. Whereas, the response time and recovery time increase obviously in the pres-

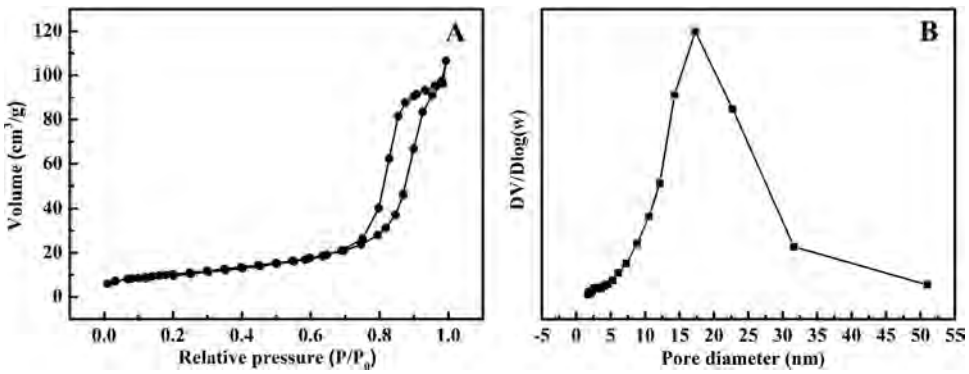

Fig. 4. (A) N_2 adsorption–desorption isotherm and (B) the corresponding BJH pore size distribution plot of Ag/Ag_2O–SnO_2—3 wt% composite.

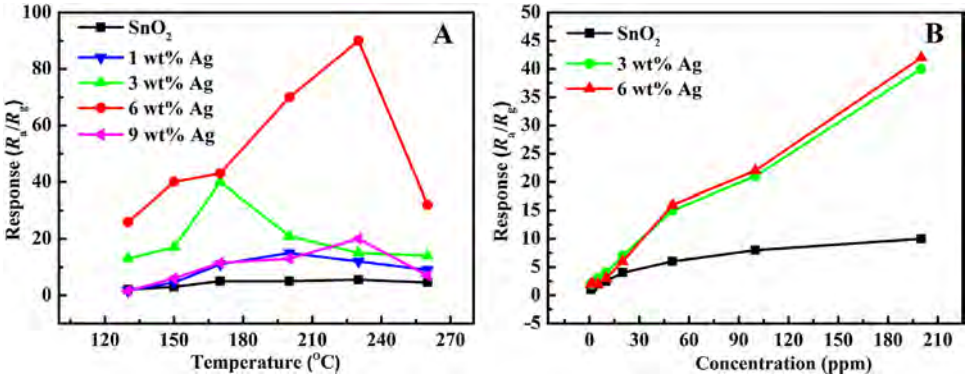

Fig. 5. (A) Response to 200 ppm hydrogen at different operating temperature for SnO_2 and Ag/Ag_2O–SnO_2 composites sensors. (B) Response to elevated concentrations of hydrogen for SnO_2, Ag/Ag_2O–SnO_2—3 wt% and Ag/Ag_2O–SnO_2—6 wt% sensors at 170 °C.

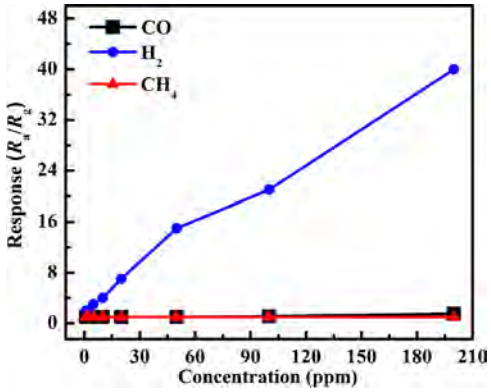

Fig. 6. Response of sensors fabricated from Ag/Ag_2O–SnO_2—3 wt% to 200 ppm different gases at 170 °C.

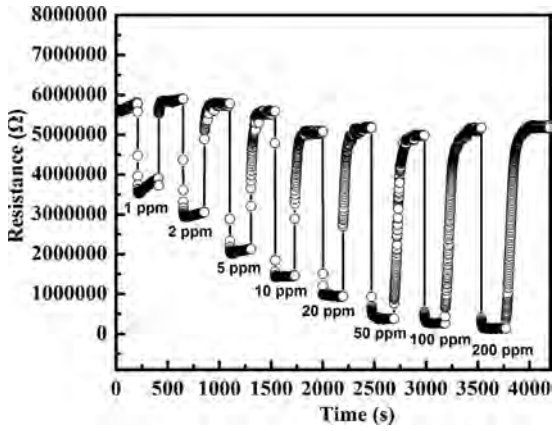

Fig. 7. Dynamic resistance curve of Ag/Ag_2O–SnO_2—3 wt% sensor to various concentrations of hydrogen at 170 °C.

ence of CO and methane due to the adsorption of these two gases on the surface of the sensing material. In this sense, this material can be used for the detection of trace hydrogen in the presence of either methane or CO or both.

The dynamic resistance of Ag/Ag_2O–SnO_2—3 wt% composite based sensor to various concentration of hydrogen (from 1 to 200 ppm) are presented in Fig. 7. The resistance decreases upon interaction with increased hydrogen concentration which is in accordance with the typical gas sensing behaviors of n-type metal oxide semiconductors [34,51].

The reproducibility and repeatability are other important factors for a gas sensing material. The reproducibility of the above

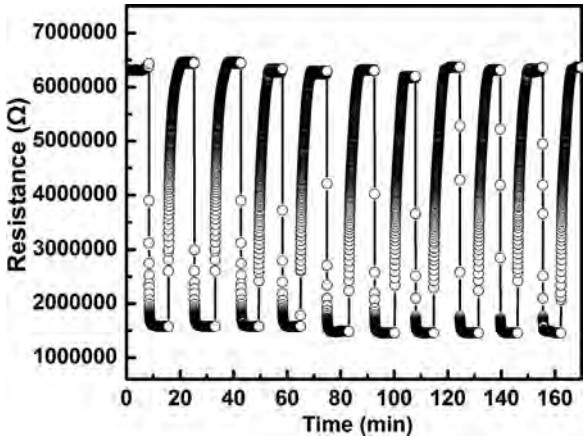

Fig. 8. The cycling performance of Ag/Ag_2O–SnO_2—3 wt% sensor at 170 °C.

sensor was studied in details. As shown in Fig. 8, the change of the resistance is identical to 20 ppm hydrogen at 170 °C for 10 times, indicating the excellent reproducibility. Furthermore, the long term stability of Ag/Ag_2O–SnO_2—3 wt% composite based gas sensor was also studied (Fig. S5). The response values were recorded every ten days for 100 days. And the responses are nearly the same, demonstrating the good stability of the material.

Ag/Ag_2O NPs functionalized porous SnO_2 exhibits high response and good selectivity at relatively low operating temperature. Both Ag/Ag_2O and SnO_2 play key roles in the enhanced gas-sensing performance. Porous SnO_2 acts as the good sensing substrate and Ag/Ag_2O further decreases the electron density on the surface of SnO_2 and improved the sensing ability. Generally, SnO_2 presents a resistance change related to a depletion layer of which the thickness is highly dependent on the adsorption and desorption of oxygen species. When SnO_2 gas senor is exposed to air, oxygen molecules can be adsorbed on the sensor surface and capture electrons from the conduction band of SnO_2 to form chemisorbed oxygen ions (O^-, O_2^- and O^{2-}). Eventually, the chemisorption process will lead to the generation of the depletion layers on the surface of sensing material, resulting in the increase of resistance. When the SnO_2 gas sensor was exposed to H_2, the chemisorbed oxygen species could react with H_2 molecules and release the electrons captured by oxygen back to SnO_2, decreasing the resistance of SnO_2 gas sensor. Furthermore, when Ag nanoparticles were decorated on the surface of the porous Ag/Ag_2O–SnO_2 microsphere, the electron transfer between Ag nanoparticles and SnO_2 microsphere should be taken into account. As we all know, the work function of Ag (Φ_s 4.72 eV) is higher than that of SnO_2 (Φ_t 4.60 eV), electrons would be favored to transfer from SnO_2 to Ag until the system reached thermodynamic

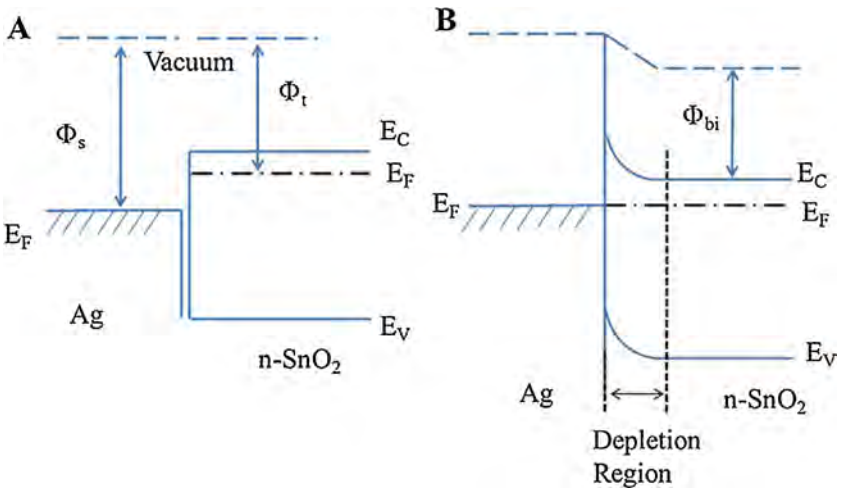

Scheme 3. Schematic illustration for the band diagram of (A) Ag and SnO_2 separately and (B) Ag decorated on SnO_2 and reached equilibrium.

equilibrium, which results in the formation of Schottky barrier at the interface between metal and semiconductor. Thus, a depletion region would be formed in SnO_2 near the interface of Ag and SnO_2 (Scheme 3B) [52–54], where E_f, E_c, E_v and Φ_{bi} are Fermi level, conduction band, valence band and work function of Ag/SnO_2 binary, respectively.

The decoration of Ag nanoparticles can further extend the electron depletion layer of SnO_2 by the electronic sensitization mechanism [55,56]. In addition, Ag_2O is a kind of *p* type semiconductor that will further extract electrons from SnO_2. And what is more, Ag/Ag_2O nanoparticles can act as active site to reduce the reaction barrier between hydrogen and the adsorbed oxygen species due to its good catalytic ability [57,58]. Generally, the Langmuir–Hinshelwood (L–H) mechanism or the Mars-van-Krevelen (MvK) mechanism or a combination of the two is usually involved in the reduction or oxidation process over the metal oxide-based materials [44,59]. In this case, the H_2 oxidation presented here should be followed a combination of L–H mechanism and MvK pathway due to the formation of Ag/Ag_2O redox couple on the surface of SnO_2. When the sensor was exposed to hydrogen, the deep electron depletion layer underneath the Ag nanoparticles would be changed into a shallow layer due to the reduction of adsorbed oxygen species, leading to a significantly enhanced gas response [55–58,60–63]. On the other hand, heavy Ag decorating would cause the electrons to conduct along the metallic Ag nanoparticles, depressing the gas sensing response [64].

At a low temperature of 170 °C, the oxidation of both CO and H_2 is hardly occurred on the surface of SnO_2 due to the high reaction barrier. Even with the help of Ag species, CO and methane can barely react with oxygen species at this temperature. In addition, CO can be absorbed on the surface of semiconductors, inactivating the sensor [65]. Thus, the porous Ag/Ag_2O–SnO_2—3 wt% composite sensor gave a response of 1.5–200 ppm CO at 170 °C (Fig. 6). And it reached 5 ppm at 250 °C (Fig. S6). With the help of Ag/Ag_2O, hydrogen could be activated on the surface of the composite, leading to the high response to hydrogen at this temperature. We believed that the proper amount of Ag species is responsible for its high response at a lower temperature. This composite material is a promising candidate for H_2 detection against CO and methane.

4. Conclusion

A composite sensing material with high response, short response time, excellent stability and good selectivity to trace hydrogen had been obtained by decorating Ag/Ag_2O nanoparticles on the surface of porous SnO_2. The as obtained Ag/Ag_2O–SnO_2—3 wt% composite gave the best hydrogen sensing performance at a relatively low working temperature of 170 °C. The enhanced sensing response and selectivity of this material could be attributed to the formation of Schottky barrier, the catalytic ability of Ag/Ag_2O nanoparticles and the low working temperature.

Acknowledgments

This work was supported by the NSFC (21371070, 21401066, 21401016); Jilin Province Science and Technology Development Projects (20150520003JH, 20140101041JC, 20130204001GX) and Key Laboratory of Functional Inorganic Material Chemistry (Heilongjiang University), Ministry of Education. Chang Yan is greatly appreciated for his help in discussion.

Appendix A. Supplementary data

Supplementary data associated with this article can be found, in the online version, at http://dx.doi.org/10.1016/j.snb.2016.01.078.

References

[1] G.A. Olah, Beyond oil and gas: the methanol economy, Angew. Chem. Int. Ed. 44 (2005) 2636–2639.
[2] K. Xie, W. Li, W. Zhao, Coal chemical industry and its sustainable development in China, Energy 35 (2010) 4349–4355.
[3] E. Shoko, B. Melellan, A.L. Dicks, J.C.D. da Costa, Hydrogen from coal: production and utilisation technologies, Int. J. Coal Geol. 65 (2006) 213–222.
[4] G.J. Stiegel, M. Ramezan, Hydrogen from coal gasification: an economical pathway to a sustainable energy future, Int. J. Coal Geol. 65 (2006) 173–190.
[5] C. Wongchoosuk, A. Wisitsoraat, D. Phokharatkul, A. Tuantranont, T. Kerdcharoen, Multi-walled carbon nanotube-doped tungsten oxide thin films for hydrogen gas sensing, Sensors 10 (2010) 7705–7715.
[6] S. Cavallaro, N. Mondello, S. Freni, Hydrogen produced from ethanol for internal reforming molten carbonate fuel cell, J. Power Sources 102 (2001) 198–204.
[7] A.L. Dicks, Molten carbonate fuel cells, Curr. Opin. Solid State Mater. Sci. 8 (2004) 379–383.
[8] P. Heidebrecht, K. Sundmacher, Molten carbonate fuel cell (MCFC) with internal reforming: model-based analysis of cell dynamics, Chem. Eng. Sci. 58 (2003) 1029–1036.
[9] Y. Wang, Z. Yuan, H. Matsuura, F. Tsukihashi, Reduction extraction kinetics of titania and iron from an ilmeniteby H_2–Ar gas mixtures, ISIJ Int. 49 (2009) 164–170.
[10] K. Sun, R. Takahashi, J. Yagi, Reduction kinetics of cement-bonded natural Ilmenite pellets with hydrogen, ISIJ Int. 32 (1992) 496–504.
[11] M.L. Vries, I.E. Grey, Influence of pressure on the kinetics of synthetic ilmenite reduction in hydrogen, Metall. Mater. Trans. B 37B (2006) 199–208.
[12] R. Merk, C.A. Pickles, Reduction of ilmenite by carbon monoxide, Can. Metall. Q. 27 (1988) 179–185.

[13] S. Itoh, A. Kikuchi, Reduction kinetics of natural ilmenite ore with carbon monoxide, Mater. Trans. 42 (2001) 1364–1372.
[14] G. Korotcenkov, S.D. Han, J.R. Stetter, Review of electrochemical hydrogen sensors, Chem. Rev. 109 (2009) 1402–1433.
[15] M. Choudhary, V.N. Mishra, R. Dwivedi, Solid-state reaction synthesized Pd-doped tin oxide thick film sensor for detection of H_2 CO, LPG and CH_4, J. Mater. Sci. 24 (2013) 2824–2832.
[16] Y. Wang, X. Jiang, Y. Xia, A solution-phase, precursor route to polycrystalline SnO_2 nanowires that can be used for gas sensing under ambient conditions, J. Am. Chem. Soc. 125 (2003) 16176–16177.
[17] S. Deng, V. Tjoa, H.M. Fan, H.R. Tan, D.C. Sayle, M. Olivo, S. Mhaisalkar, J. Wei, C.H. Sow, Reduced graphene oxide conjugated Cu_2O nanowire mesocrystals for high-performance NO_2 gas sensor, J. Am. Chem. Soc. 134 (2012) 4905–4917.
[18] L.K. Bagal, J.Y. Patil, M.V. Vaishampayan, I.S. Mulla, S.S. Suryavanshi, Effect of Pd and Ce on the enhancement of ethanol vapor response of SnO_2 thick films, Sens. Actuators B 207 (2015) 383–390.
[19] C. Wang, X. Li, C. Feng, Y. Sun, G. Lu, Nanosheets assembled hierarchical flower-like WO_3 nanostructures: synthesis characterization, and their gas sensing properties, Sens. Actuators B 210 (2015) 75–81.
[20] X.-L. Li, T.-J. Lou, X.-M. Sun, Y.-D. Li, Highly sensitive WO_3 hollow-sphere gas sensors, Inorg. Chem. 43 (2004) 5442–5449.
[21] R.C. Pawar, J.S. Shaikh, A.V. Moholkar, S.M. Pawar, J.H. Kim, J.Y. Patil, S.S. Suryavanshi, P.S. Patil, Surfactant assisted low temperature synthesis of nanocrystalline ZnO and its gas sensing properties, Sens. Actuators B 151 (2010) 212–218.
[22] B.T. Waitz, T. Wagner, T. Sauerwald, C.-D. Kohl, M. Tiemann, Ordered mesoporous In_2O_3: synthesis by structure replication and application as a methane gas sensor, Adv. Funct. Mater. 19 (2009) 653–661.
[23] B. Dalkiran, C. Kaççar, P.E. Erden, E. Kiliç, Amperometric xanthine biosensors based on chitosan-Co_3O_4-multiwall carbon nanotube modified glassy carbon electrode, Sens. Actuators B 200 (2014) 83–91.
[24] Y. Cao, J. Zhao, X. Zou, P.-P. Jin, H. Chen, R. Gao, L.-J. Zhou, Y.-C. Zou, G.-D. Li, Synthesis of porous In_2O_3 microspheres as a sensitive material for early warning of hydrocarbon explosions, RSC Adv. 5 (2015) 5424–5431.
[25] A. Martucci, N. Bassiri, M. Guglielmi, NiO-SiO_2 sol-gel nanocomposite films for optical gas sensor, J. Sol-Gel Sci. Technol. 26 (2003) 993–996.
[26] J. Park, X. You, Y. Jang, Y. Nam, M.J. Kim, N.K. Min, J.J. Pak, ZnO nanorod matrix based electrochemical immunosensors for sensitivity enhanced detection of *Legionellaa pneumophil*, Sens. Actuators B 200 (2014) 173–180.
[27] J. Li, H. Fan, X. Jia, Multilayered ZnO nanosheets with 3D porous architectures: synthesis and gas sensing application, J. Phys. Chem. C 114 (2010) 14684–14691.
[28] J. Zhao, X. Zou, L.-J. Zhou, L.-L. Feng, P.-P. Jin, Y.-P. Liu, G.-D. Li, Precursor-mediated synthesis and sensing properties of wurtzite ZnO microspheres composed of radially aligned porous nanorods, Dalton Trans. 42 (2013) 14357–14360.
[29] A. Bejaoui, J. Guerin, J.A. Zapien, K. Aguir, Theoretical and experimental study of the response of CuO gas sensor under ozone, Sens. Actuators B 190 (2014) 8–15.
[30] J. Gong, Y. Li, Z. Hu, Z. Zhou, Y. Deng, Ultrasensitive NH_3 gas sensor from polyaniline nanograin enchased TiO_2 fibers, J. Phys. Chem. C 114 (2010) 9970–9974.
[31] P.C. Pawar, J. Lee, V.B. Patil, C.S. Lee, Synthesis of multi-dimensional ZnO nanostructures in aqueous medium for the application of gas sensor, Sens. Actuators B 187 (2013) 323–330.
[32] K. Xu, D. Zeng, S. Tian, S. Zhang, C. Xie, Hierarchical porous SnO_2 micro-rods topologically transferred from tin oxalate for fast response sensors to trace formaldehyde, Sens. Actuators B 190 (2014) 585–592.
[33] Y. Liu, Y. Jiao, Z. Zhang, F. Qu, A. Umar, X. Wu, Hierarchical SnO_2 nanostructures made of intermingled ultrathin nanosheets for environmental remediation smart gas sensor, and supercapacitor applications, ACS Appl. Mater. Interfaces 6 (2014) 2174–2184.
[34] P.-P. Jin, X. Zou, L.-J. Zhou, J. Zhao, H. Chen, Y. Tian, G.-D. Li, Biopolymer-assisted construction of porous SnO_2 microspheres with enhanced sensing properties, Sens. Actuators B 204 (2014) 142–148.
[35] Z. Wang, Z. Li, J. Sun, H. Zhang, W. Wang, W. Zheng, C. Wang, Improved hydrogen monitoring properties based on *p*-NiO/*n*-SnO_2 heterojunction composite nanofibers, J. Phys. Chem. C 114 (2010) 6100–6105.
[36] D. Kohl, Surface processes in the detection of reducing gases with SnO_2-based devices, Sens. Actuators B 18 (1989) 71–113.
[37] J. Huang, N. Matsunaga, K. Shimanoe, N. Yamazoe, T. Kunitake, Nanotubular SnO_2 templated by cellulose fibers: synthesis and gas sensing, Chem. Mater. 17 (2005) 3513–3518.
[38] J. Zhang, B.K. Miremadi, K. Colbow, Effects of surface silver additives on tin oxide thin film gas sensors, J. Mater. Sci. Lett. 13 (1994) 1048–1050.
[39] J. Zhang, K. Colbow, Surface silver clusters as oxidation catalysts on semiconductor gas sensors, Sens. Actuators B 40 (1997) 47–52.
[40] N. Yamazoe, Y. Kurokawa, T. Seiyama, Hydrogen sensitive gas detector using silver added tin(IV) oxide, Chem. Lett. (1982) 1899–1902.
[41] A. Abdel-Wahab, O. Mohamed, S. Ahmed, M. Mostafa, Ag-doped TiO_2 enhanced photocatalytic oxidation of 1,2-cyclohexanediol, J. Phys. Org. Chem. 25 (2012) 1418.
[42] A.M. Ferraria, A.P. Carapeto, A.M.B. do Rego, X-ray photoelectron spectroscopy: silver salts revisited, Vacuum 86 (2012) 1988–1991.
[43] M. Rocca, L. Savio, L. Vattuone, U. Burghaus, V. Palomba, N. Novelli, F. Buatier de Mongeot, U. Valbusa, Phase transition of dissociatively adsorbed oxygen on Ag (0 0 1), Phys. Rev. B 61 (2000) 213–227.
[44] S.K. Megarajan, S. Rayalu, M. Nishibori, Y. Teraoka, N. Labhsetwar, Effects of surface and bulk silver on $PrMnO_{3+\delta}$ perovskite for CO and soot oxidation: experimental evidence for the chemical state of silver, ACS Catal. 5 (2015) 301–309.
[45] S.S. Acharyya, S. Ghosh, R. Bal, Fabrication of three dimensional (3D) hierarchical Ag/WO_3 flower-like catalyst materials for the selective oxidation of m-xylene to isophthalic acid, Chem. Commun. 51 (2015) 5998–6001.
[46] X. Xiao, G. Xu, B. Xiong, D. Chen, L. Miao, The film thickness dependent thermal stability of Al_2O_3: Ag thin films as high-temperature solar selective absorbers, J. Nanopart. Res. 14 (2012) 746–756.
[47] H. Zhang, Q. He, X. Zhu, D. Pan, X. Deng, Z. Jiao, Surfactant-free solution phase synthesis of monodispersed SnO_2 hierarchical nanostructures and gas sensing properties, CrystEngComm 14 (2012) 3169–3176.
[48] Y.-T. Wang, W.-T. Whang, C.-H. Chen, Hollow V_2O_5 nanoassemblies for high-performance room-temperature hydrogen sensors, ACS Appl. Mater. Interfaces 7 (2015) 8480–8487.
[49] M. Tiemann, Porous metal oxides as gas sensors, Chem. Eur. J. 13 (2007) 8376–8388.
[50] J. Zhang, S. Wang, M. Xu, Y. Wang, B. Zhu, S. Zhang, W. Huang, S. Wu, Hierarchically porous ZnO architectures for gas sensor application, Cryst. Growth Des. 9 (2009) 3532–3537.
[51] Q. Qi, P.-P. Wang, J. Zhao, L.-L. Feng, L.-J. Zhou, R.-F. Xuan, Y.-P. Liu, G.-D. Li, SnO_2 nanoparticle-coated In_2O_3 nanofibers with improved NH_3 sensing properties, Sens. Actuators B 194 (2014) 440–446.
[52] M. Schnippering, M. Carrara, A. Foelske, R. Kotz, D.J. Fermn, Electronic properties of Ag nanoparticle arrays. A Kelvin probe and high resolution XPS study, Phys. Chem. Chem. Phys. 9 (2007) 725–730.
[53] L. Wang, H. Dou, Z. Lou, T. Zhang, Encapsuled nanoreactors (Au@SnO_2): a new sensing material for chemical sensors, Nanoscale 5 (2013) 2686–2691.
[54] Y. Harima, H. Okazaki, Y. Kunugi, K. Yamashita, H. Ishii, K. Seki, Formation of Schottky barriers at interfaces between metals and molecular semiconductors of p- and n-type conductances, Appl. Phys. Lett. 68 (1996) 1059–1061.
[55] I. Hwang, J. Choi, H. Woo, S. Kim, S. Jung, T. Seong, I. Kim, J. Lee, Facile control of C_2H_5OH sensing characteristics by decorating discrete Ag nanoclusters on SnO_2 nanowire networks, ACS Appl. Mater. Interfaces 3 (2011) 3140–3145.
[56] J. Wang, B. Zou, S. Ruan, J. Zhao, F. Wu, Synthesis characterization, and gas-sensing property for HCHO of Ag-doped In_2O_3 nanocrystalline powders, Mater. Chem. Phys. 117 (2009) 489–493.
[57] S. Choi, A. Katoch, J. Kim, S.S. Kim, Prominent reducing gas-sensing performances of n-SnO_2 nanowires by local creation of p-n heterojunctions by functionalization with p-Cr_2O_3 nanoparticles, ACS Appl. Mater. Interfaces 6 (2014) 17723–17729.
[58] H. Kim, K. Choi, K. Kim, I. Kim, G. Cao, J. Lee, Ultra-fast responding and recovering C_2H_5OH sensors using SnO_2 hollow spheres prepared and activated by Ni templates, Chem. Commun. 46 (2010) 5061–5063.
[59] N. Yamazoe, New approaches for improving semiconductor gas sensors, Sens. Actuators B 5 (1991) 7–19.
[60] W. Zeng, T.-M. Liu, D.-J. Liu, Formaldehyde gas sensing property and mechanism of TiO_2–Ag nanocomposite, Phys. B 405 (2010) 4235–4239.
[61] P. Hu, G. Du, W. Zhou, J. Cui, J. Lin, H. Liu, D. Liu, J. Wang, S. Chen, Enhancement of ethanol vapor sensing of TiO_2 nanobelts by surface engineering, ACS Appl. Mater. Interfaces 2 (2010) 3263–3269.
[62] V.N. Singh, B.R. Mehta, R.K. Joshi, F.E. Kruis, S.M. Shivaprasad, Enhanced gas sensing properties of In_2O_3:Ag composite nanoparticle layers; electronic interaction, size and surface induced effects, Sens. Actuators B 125 (2007) 482–488.
[63] S. Matsushima, Y. Teraoka, N. Miura, N. Yamazoe, Electronic interaction between metal additives and tin dioxide in tin dioxide-based gas sensors, Jpn. J. Appl. Phys. 27 (1988) 1798–1802.
[64] M. Horprathum, T. Srichaiyaperk, B. Samransuksamer, A. Wisitsoraat, P. Eiamchai, S. Limwichean, C. Chananonnawathorn, K. Aiempanakit, N. Nuntawong, V. Patthanasettakul, C. Oros, S. Porntheeraphat, P. Songsiriritthigul, H. Nakajima, A. Tuantranont, P. Chindaudom, Ultrasensitive hydrogen sensor based on Pt-decorated WO_3 nanorods prepared by Glancing-Angle dc magnetron sputtering, ACS Appl. Mater. Interfaces 6 (2014) 22051–22060.
[65] R.K. Herz, CO-oxidation catalysts: low-temperature CO oxidation over noble-metal reducible-oxide (NMRO) catalysts, J. Catal. 141 (1993) 219–238.

Biographies

Hui-Hui Li is a master student in State Key Laboratory of Inorganic Synthesis & Preparative Chemistry, Jilin University in China. Her research interest is the synthesis of sensing nanomaterials.

Yi He is a full professor at College of Chemistry, Jilin University in China. She received PhD (2006) from Jilin University. Her research interests in preparation and characterization of inorganic-organic hybrid materials.

Pan-Pan Jin is a master student in State Key Laboratory of Inorganic Synthesis & Preparative Chemistry, Jilin University in China. Her research interest is the synthesis of sensing nanomaterials.

Yang Cao is a currently a Ph.D candidate in State Key Laboratory of Inorganic Synthesis & Preparative Chemistry, Jilin University in China. His research interest is the synthesis of sensing nanomaterials.

Mei-Hong Fan is a master student in State Key Laboratory of Inorganic Synthesis & Preparative Chemistry, Jilin University in China. Her research interest is the design and synthesis of noble metal-free, nanostructured and/or nanoporous materials.

Xiaoxin Zou was awarded a Ph.D. in Inorganic Chemistry from Jilin University (China) in 06/2011; and then moved to the University of California, Riverside and Rutgers, The State University of New Jersey as a Postdoctoral Scholar from 07/2011 to 10/2013. He is currently an associate professor in Jilin University. His research interests focus on the design and synthesis of noble metal-free, nanostructured and/or nanoporous materials for water splitting and renewable energy applications.

Guo-Dong Li is a full professor at State Key Lab of Inorganic Synthesis & Preparative Chemistry, College of Chemistry, Jilin University in China. He received his B.Sc. (1995), M.Sc (1998) and PhD (2001) from Jilin University. His research interests include chemical sensors, lithium batteries, photocatalysts.